Catalysis Today 155 (2010) 140–146

Contents lists available at ScienceDirect

Catalysis Today

journal homepage: www.elsevier.com/locate/cattod

Influence of aging effects on the conversion efficiency of automotive exhaust gas catalysts

Alexander Winkler [a,*], Davide Ferri [b], Roland Hauert [c]

[a] Empa, Swiss Federal Laboratories for Materials Testing and Technology, Internal Combustion Engines Laboratory, Ueberlandstrasse 129, CH-8600 Duebendorf, Switzerland
[b] Empa, Swiss Federal Laboratories for Materials Testing and Technology, Laboratory for Solid State Chemistry and Catalysis, Ueberlandstrasse 129, 8600 Duebendorf, Switzerland
[c] Empa, Swiss Federal Laboratories for Materials Testing and Technology, Laboratory for Nanoscale Materials Science, Ueberlandstrasse 129, 8600 Duebendorf, Switzerland

ARTICLE INFO

Article history:
Available online 10 January 2009

Keywords:
Commercial automotive catalysts
Three-way catalysts
Diesel oxidation catalysts
Bifuel vehicle
Aging
Activity
XPS
SEM
EDX
BET

ABSTRACT

The influence of chemical and thermal aging effects on catalytic activity was analyzed for a vehicle (bifuel) aged pre- and underfloor three-way catalyst (p-/u-TWC) as well as an engine aged diesel oxidation catalyst (DOC). The conversion results were compared with the respective new catalysts. Although the vehicle aged p-TWC showed massive thermal aging, its CO conversion rate was comparable to that of the vehicle aged u-TWC. On the other hand, the conversion rate for methane abatement was significantly affected above 325 °C. Methane conversion appeared as the parameter mostly affected by (thermal) aging. The DOC showed massive chemical aging with typical engine oil based contaminants like P and Zn but also with Si. The contamination is likely responsible for the shift of propene and NO light-off curves to higher temperatures by about 70 °C.

1. Introduction

Long-term compliance with automotive exhaust gas emission regulations is one of the challenges faced by the automotive industry. Although both three-way catalysts (TWC) and diesel oxidation catalysts (DOC) have proven to be efficient even after high mileage, new issues have been raised. Increasingly stringent emission standards (e.g. Euro 5 in September 2009) require the catalysts to be more efficient and aging resistant. New fuel concepts (e.g. compressed natural gas, CNG) and engine designs (e.g. direct injection for gasoline, engine down-sizing) influence the exhaust gas composition and temperature which can cause accelerated catalyst aging. Furthermore, the impact of different catalyst aging phenomena on the conversion efficiency can change, too. One example is the methane selective TWC deactivation. It results in unburned hydrocarbon emission (THC), consisting mainly of methane, above the allowed limiting value but only when CNG is used as fuel [1,2].

For both TWCs and DOCs chemical and thermal aging effects are the primary sources for catalyst deactivation. Chemical aging compounds mostly originate from engine oil additives. Additives functioning as detergents (e.g. metal sulfonates) contain alkaline earth metals, primarily Ca and Mg. Zinc-dialkyldithiophosphates (ZnDDP) are commonly used as wear reducing and aging stability increasing additives and contain Zn, P and S. Anti-foaming additives can be based on silicon containing compounds [3,4]. These contaminants cause fowling of the washcoat surface. Additionally some contaminants directly interact with the precious metals and the oxides of the washcoat compounds. Thermal aging effects can cause sintering of PM particles and the washcoat itself, thus reducing its catalytic efficiency [5–9]. Establishing a relationship between a certain aging effect and the resulting influence on the automotive catalyst conversion for a certain exhaust gas compound is challenging. In case of real, vehicle aged automotive catalysts the complexity of the system increases even further [10,11].

This paper presents results about the influence of chemical and thermal aging effects on the catalytic activity of automotive exhaust gas catalysts. A pre- and underfloor-TWC, both road-aged in the same bifuel (gasoline/CNG) passenger car for 35,000 km, and

* Corresponding author. Tel.: +41 44 823 4333; fax: +41 44 823 4044.
E-mail address: alexander.winkler@empa.ch (A. Winkler).

Abbreviations: BET, Brunauer, Emmett, Teller; CNG, compressed natural gas; DOC, diesel oxidation catalyst; EDX, energy dispersive X-ray spectrometry; MS, mass spectrometry; PM, precious metal; SEM, scanning electron microscopy; SSA, specific surface area; THC, total hydrocarbons; p-TWC, pre three-way catalyst; u-TWC, underfloor three-way catalyst; XPS, X-ray photoelectron spectroscopy.

0920-5861/$ – see front matter © 2008 Elsevier B.V. All rights reserved.
doi:10.1016/j.cattod.2008.11.021

a DOC, engine aged on a test bench, were analyzed. XPS was used to identify and to quantify the different chemical aging compounds on all catalyst surfaces. Their distribution on the surface was characterized via EDX mappings, the depth distribution was determined employing sputter depth profiling. Thermal aging effects were identified using SEM/EDX and BET. The catalytic activities were monitored in a conventional flow reactor equipped with an MS, using a simplified and a more realistic exhaust gas for the TWCs and the DOC, respectively. For comparison, a new p-TWC, u-TWC and DOC of the same type were analyzed as well.

The work presented in [2] focused on the origin of the selective loss of methane conversion on TWC. Detailed XPS studies suggested that changes in the state of the Pd active phase determine the loss of methane conversion. Chemical and thermal aging effects were only briefly addressed. Here, a detailed quantitative analysis of all chemical aging compounds, including their depth distribution, is presented. Additionally, SEM/EDX mappings provide answers about the composition and spatial distribution of contaminants detected in the overlayer. SEM/EDX mappings also allowed for a thorough analysis of thermal aging effects, providing information about sintered precious metal particle size and distribution. Finally, the influences of the aging effects on the catalytic activity have been assessed in a model reactor using model exhaust gases.

2. Experimental

The pre-TWC (p-TWC) and the underfloor-TWC (u-TWC) originate from the same commercially available serial production bifuel passenger car of a European OEM. The p-TWC was installed in close vicinity to the engine; the u-TWC was installed farther downstream in the exhaust gas path. The catalysts were vehicle aged for 35,000 km (roughly corresponding to 800 h) on the road during everyday use of the car.

Both catalysts consisted of a cordierite monolith carrier with applied washcoat. According to manufacturers' instruction, the total PM content of the p-TWC was 75 g/ft^3. It contained Pt, Pd and Rh in different concentrations with the Pd content being the highest. The PM content of the u-TWC amounted to 250 g/ft^3 with predominantly Pd and minor amounts of Pt.

The DOC only contained Pt as catalytically active species; information about the PM content was not available.

All aged catalyst samples were taken from center area of the exhaust gas entrance, whereas the samples of the new catalysts were taken from the middle. For XPS and SEM/EDX analysis rectangular pieces about 2 mm × 5 mm × 10 mm in size have been carefully cut out from the respective catalyst.

XPS spectra were acquired on a Physical Electronics (PHI) Quantum 2000 photoelectron spectrometer using monochromated AlKα radiation and a hemispherical capacitor electron-energy analyzer equipped with a channel plate and a position-sensitive detector. The electron take-off angle was 45° and the analyzer was operated in the constant pass energy mode (117.4 eV, calibrated to a total analyzer energy resolution of 1.62 eV for Ag 3d electrons) for all measurements. The beam diameter was typically 100 μm, thus allowing analyzing only the washcoat covered monolith channel. Special care was taken to avoid the uncovered wall fractures during analysis.

Sputtering was performed with Ar^+; the acceleration energy was 4 kV. 36 s of sputtering resulted in a depth of about 10 nm.

Quantitative analysis was performed employing PHI MultiPak V6.1A. The C 1 s signal position at 284.8 eV binding energy (BE) was used as an internal standard for calibration of the XP-signal positions. In case of sputtered samples, the Ar 2p signal position at 243.0 eV BE was used for calibration [13].

SEM images were recorded on a high resolution Hitachi S-4800 SEM employing an acceleration voltage of 7 kV, a work distance of 15 mm and an upper secondary electron detector. The magnification of all images was ×5000. For EDX mappings an Oxford Instruments INCAPentaFET-x3 detector and the INCAEnergy Microanalysis software were used. Measuring parameters were 7 kV acceleration voltage, 15 mm work distance, 15 μA beam current, activated site lock. All samples were glued to the sample holder using a conductive carbon solution and coated via carbon thread evaporation.

Dynamic single point BET analysis was performed on a Chembet-3000 from Quantachrome Instruments, employing a gas mixture containing 30.21 mol% nitrogen in helium. All catalyst samples were ground in an agate mortar and, prior to analysis, baked out for 2 h at 200 °C under a nitrogen flow.

For catalytic tests, 0.8 g of grinded and sieved (150–200 μm granules) catalyst were placed between two quartz wool plugs in a conventional quartz reactor (d_i = 12 mm) operated at ambient pressure, which was heated by an electric furnace. The temperature was measured using a thermocouple installed on the external wall of the reactor in correspondence of the catalyst bed. The new TWCs were degreened in a muffle furnace at 800 °C for 4 h in ambient air. Prior to reaction, all catalysts were oxidized in the reactor at 500 °C for 1 h in synthetic air at a flow rate of 200 ml/min. Then, the catalysts were cooled in this atmosphere to the starting temperature of the reaction (TWC: 30 °C, DOC: 150 °C). The following gas mixtures were used (200 ml/min flow rate) for the respective catalyst. (a) TWC: 2000 ppm CH_4, 8500 ppm CO, 3 vol.% O_2 with balance He. (b) DOC: 1200 ppm C_3H_6, 300 ppm C_3H_8, 3000 ppm CO, 250 ppm NO, 25 vol.% CO_2, 11 vol.% O_2, balance N_2.

The TWC catalysts were tested in the temperature range 30–800 °C with a 10 °C/min heating rate, whereas the DOC catalysts were tested between 150 and 600 °C at the same heating rate. The composition of the gas stream at the outlet of the reactor was analyzed using a mass spectrometer (Balzers Omnistar) and results are expressed in terms of CH_4 (m/z 15) and CO (m/z 28) (TWC), and NO (m/z 30) and propene (m/z 42) (DOC) conversions.

3. Results and discussion

Sections 3.1 and 3.2 will focus on the discussion of different aging effects and on their influence on the catalytic performance of the vehicle aged p- and u-TWC and of the engine aged diesel oxidation catalyst, respectively.

3.1. Three-way catalysts

Fig. 1 shows SEM images (×5000) and EDX mappings of the new (a and b) and vehicle aged (c and d) p-TWC surface. The surface morphology of new TWCs as well as DOCs generally resembles the one shown in Fig. 1a. The EDX mapping of the new p-TWC surface (Fig. 1b) shows the two primary washcoat components. The red areas correspond to Al (alumina); the green areas are related to Zr (zirconia). The small blue dots correspond to palladium and hint to a homogenous Pd-distribution within the analyzed area. Fig. 1c shows an SEM image of the vehicle aged p-TWC surface morphology. The amount of clearly discernable islands is drastically reduced; the surface roughness seems to have increased. Furthermore, the surface seems to be fused together. This hints to thermal induced sintering which is confirmed by the BET analysis data shown in Table 1. The specific surface area (SSA) of the new p-TWC amounts to 42 m^2/g, whereas it is only 3 m^2/g in case of the vehicle aged p-TWC. For comparison, the SSA of the u-TWC is reduced from 43 to 23 m^2/g. Keeping in mind that the p-TWC was designed to endure high temperatures and that the

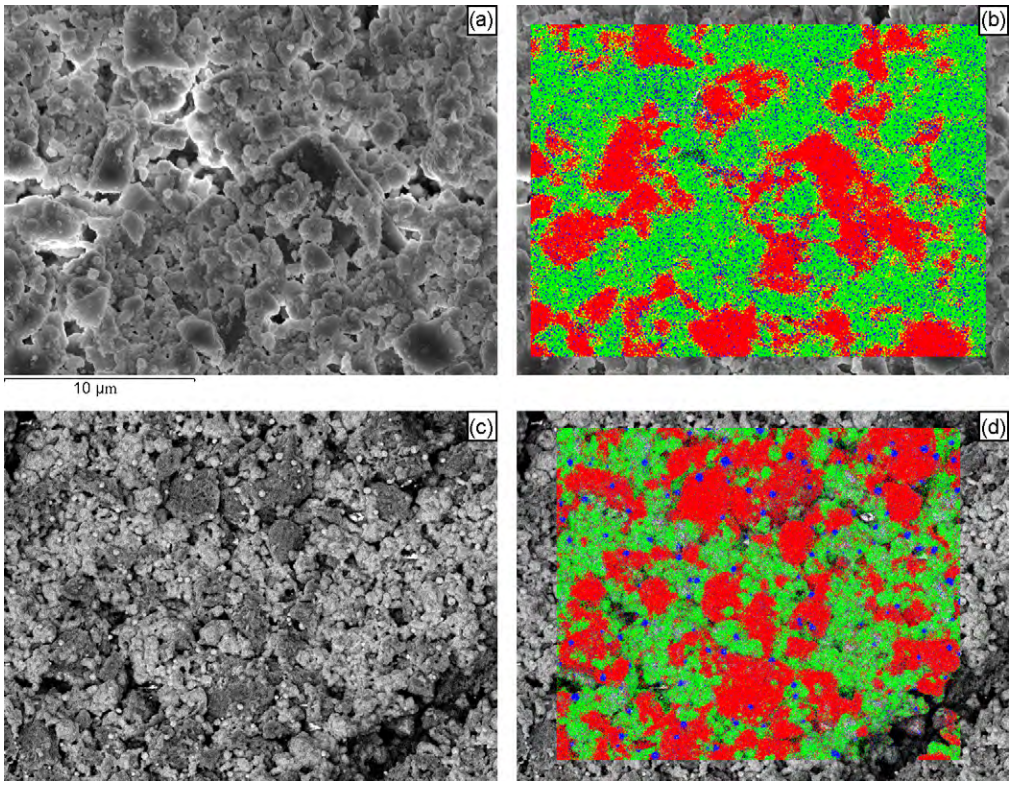

Fig. 1. SEM images of the new (a) and vehicle aged (c) p-TWC. EDX mappings of the respective areas are shown in (b) and (d). Color code (b) and (d): Al: red, Zr: green, Pd: blue.

exhaust gas temperature of a gasoline engine can reach 900 °C under regular operation, the catalyst must have been exposed to massive thermal stress.

Another interesting effect most likely based on very high temperatures is shown in the EDX mapping, Fig. 1d (Al: red, Zr: green, Pd: blue). The Pd particles are clearly visible for the vehicle aged p-TWC and have formed large, spherical clusters with diameters up to a couple of hundred nanometers. Typically, the Pd particle size in case of new TWCs is two orders of magnitude smaller.

The loss of SSA in case of the vehicle aged u-TWC was much smaller (Table 1) and no Pd particle agglomeration was detected in the SEM/EDX.

Typical contaminants as well as their concentration detected on the p- and u-TWC surfaces are given in Table 2. The carbon concentration detected on both TWCs is not above the typical hydrocarbon pollution due to storage of the sample in ambient air. P, Ca and Mg primarily originate from the lubricating oil; both the new and old engine oil was analyzed and contained significant amounts of these elements. It is interesting to note that in case of the u-TWC phosphorous is the highest concentrated contaminant whereas in case of the p-TWC it could not be detected by XPS. The reason for the absence of P on the p-TWC is unclear. But since both catalysts originate from the same exhaust aftertreatment system and only the p-TWC showed massive thermal damage (Fig. 1d and Table 1), the phenomenon is probably related to the excessive heat experienced by the p-TWC.

The source of Si, which was detected on both TWC surfaces, is unclear. According to oil analysis, neither the new nor the old engine oil contained significant amounts of Si. These sources can therefore be excluded. The new TWCs of the same type also did not include Si. With respect to the fuel, neither CNG (additive free except for S containing odorants) nor the additives used in gasoline contain Si [4]. A possible source might have been small SiO_2-containing dust particles which passed the air intake filter. According to Rokosz et al. [6] Si might also originate from silicone elastomer engine sealants, which could have been dissolved up to a certain degree by the phosphorous containing engine oil. Furthermore, the ceramic cordierite carrier is partly composed of Si ($2MgO{\cdot}2Al_2O_3{\cdot}5SiO_2$), although cordierite is thermally stable up to 1450 °C.

Fig. 2 shows that the distribution pattern of Si is different for each aged TWC. In case of the p-TWC (Fig. 2a, Al: red, Si: green), Si islands seem to be evenly distributed over the whole surface analyzed. This distribution pattern resembles that of the washcoat

Table 1
Specific surface areas of the new and vehicle aged p- and u-TWC as well as the engine aged DOC.

Catalyst	Specific surface area [m^2/g]	
	New	Aged
p-TWC	42	3
u-TWC	43	23
DOC	39	49

Table 2
Contaminant concentrations detected on the vehicle aged p- and u-TWC as well as the engine aged DOC. "Washcoat" concentration refers to all elements belonging to the washcoat of the TWCs and DOC, respectively. Balance to 100%: Oxygen.

Element	Contaminant concentration [atom%]		
	p-TWC	u-TWC	DOC
Phosphorous	–	6.1	7.2
Silicon	7.0	3.5	9.2
Calcium	1.6	2.2	1.0
Magnesium	1.8	1.2	3.2
Zinc	–	–	3.9
Iron	–	–	2.2
Carbon	8.9	8.0	17.3
Washcoat	21.7	24.3	2.8

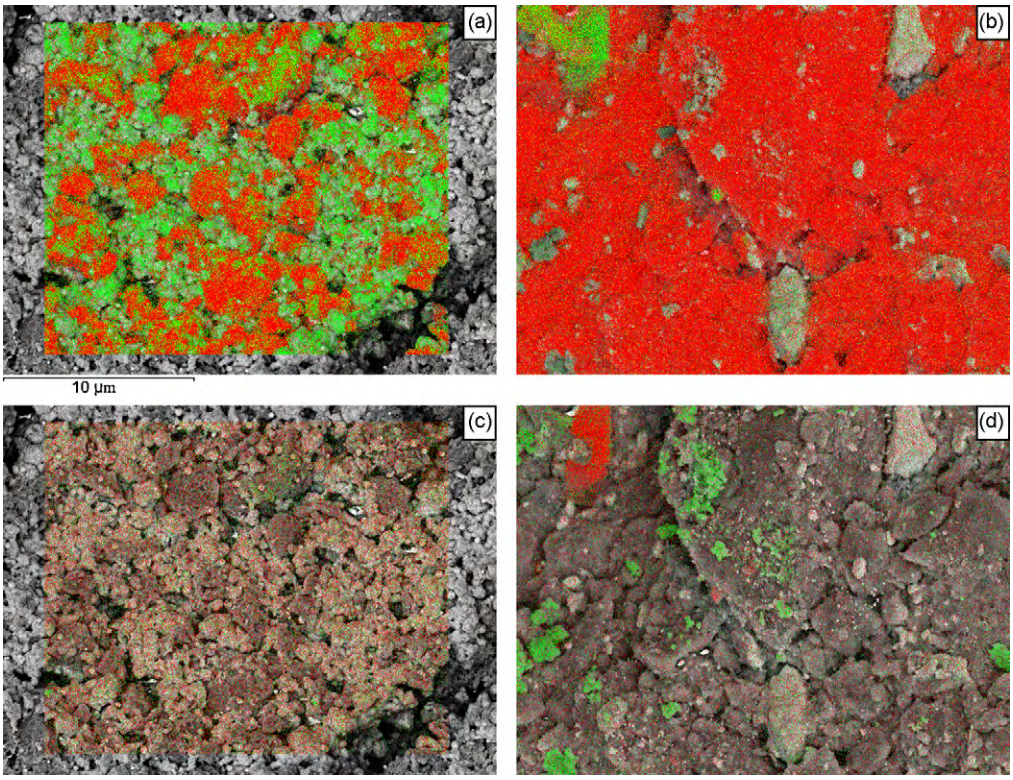

Fig. 2. SEM/EDX mappings of the vehicle aged p-TWC (a and c) and vehicle aged u-TWC (b and d). Color code (a) and (b): Al: red, Si: green. Color code (c) and (d): Mg: red, Ca: green. Simultaneous signal detection of both respective elements: yellow.

compound Zr (Fig. 1d, green areas). In case of the vehicle aged u-TWC (Fig. 2b, Al: red, Si: green) Si is much more localized. Its distribution resembles that of Ca and Mg (Fig. 2d, Mg: red, Ca: green) both of which form localized, non-uniformly distributed islands on the u-TWC surface. This hints to Si being deposited on the surface via the exhaust gas; diffusion from the cordierite is very unlikely. Nevertheless, the exact source of Si, e.g. dissolved silicone containing engine sealant elastomers or dust could not be identified.

The explanation for the different Si distribution in case of the p-TWC can most likely be attributed to the exceptionally high temperatures experienced by this catalyst. Si deposited via the exhaust gas might have diffused over the washcoat surface causing a more homogenous distribution. The almost statistical distribution of Mg and Ca on the aged p-TWC surface (Fig. 2c, Mg: red, Ca: green) seems to confirm this hypothesis. In addition to the possible Si sources discussed above, it cannot be excluded that Si might have diffused from the cordierite to the p-TWC surface due to the very high temperatures. Angove et al. [12] analyzed the effect of temperature on a ceria-baria-alumina coated cordierite monolith employing XRD. After high temperature aging up to 1200 °C for 3 h in reducing atmosphere the authors detected a new, Mg containing hexa-aluminate phase. According to the authors the only possible Mg source was the cordierite carrier. Although the authors did not mention Si, only XRD was used to characterize the surface, it nevertheless shows that diffusion of cordierite compounds is possible after a relatively short amount of time at temperatures well below the cordierite decomposition temperature. In case of the p-TWC the massive sintering also hints to temperatures in this regime, the SSA loss is comparable to the one measured by Angove et al. [12], and the exhaust gas also provides a reducing environment during rich cycles.

Fig. 3 shows the activity data of the TWC catalysts with respect to methane and CO abatement. All TWCs, even the vehicle aged p-TWC, displayed a CO conversion at ambient temperature, before the measurement started. Therefore, the final CO conversion displayed in Fig. 3 only reaches a maximum of ca. 90%.

It is remarkable that the dramatic SSA loss observed for the p-TWC did not result in its complete deactivation. Instead, it still is catalytically active towards both CO and methane. The loss in activity towards CO is even comparable with the one observed for the vehicle aged u-TWC, even though the latter (a) retained a much higher SSA and (b) contains much more PM. In both cases the light-off temperatures are by about 110 °C higher than those of the degreened samples (Table 3). Nevertheless, the maximum attainable CO conversion of the p-TWC does seem to be lower compared to both the degreened p-TWC and the vehicle aged u-TWC (Fig. 3). Furthermore the CO conversion in case of the u-TWC increases at about 110 °C, whereas in case of the p-TWC it increases at 160 °C.

Contrary to CO, a substantial effect of aging on the conversion rate of methane can be observed. While the catalytic activity remains substantially intact in case of the aged u-TWC, abatement of methane appears more difficult for the aged p-TWC despite the very close light-off temperature to that of the degreened p-TWC.

Table 3
Light-off temperatures (T_{50}) of TWC samples for CO and CH_4 conversion and of DOC samples for NO and propene conversion. For NO conversion, the temperature of maximum conversion is reported together with the conversion value (%).

Catalyst	Light-off temperature, T_{50} [°C]			
	CO	CH_4	NO	C_3H_6
p-TWC, degr.	77	319	–	–
p-TWC, aged	184	335	–	–
u-TWC, degr.	62	284	–	–
u-TWC, aged	177	310	–	–
DOC, new	–	–	215–260 (41)	175
DOC, aged	–	–	251 (32)	244

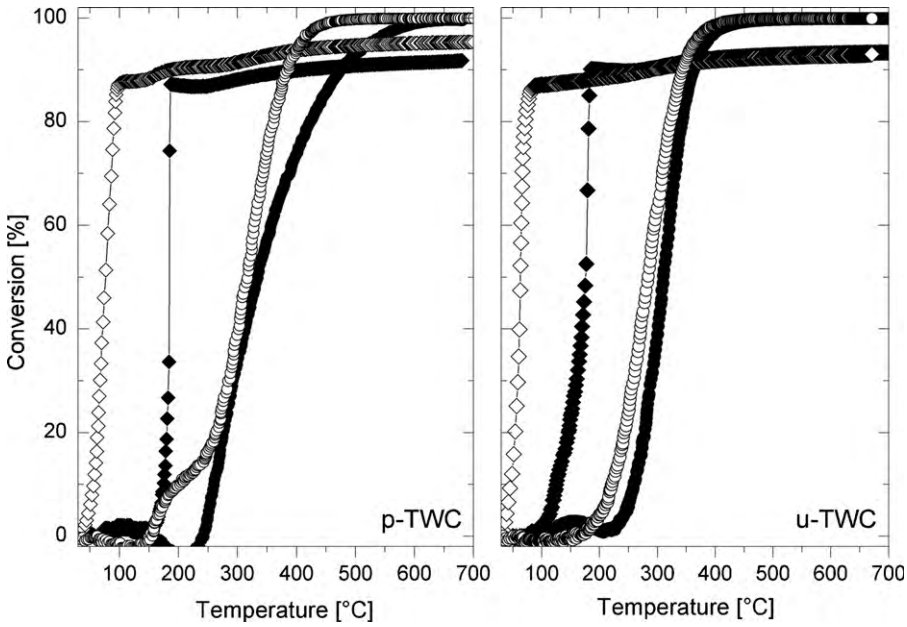

Fig. 3. Catalytic activity data for (left) p-TWC and (right) u-TWC for methane (○) and CO (◇) conversion. Open and filled symbols represent degreened and aged catalysts, respectively.

The aged p-TWC exhibits lower activity than the degreened p- and u-TWCs above 325 °C. Full conversion is attained only at 650 °C compared to 400 and 500 °C for the degreened u-TWC and p-TWC samples, respectively.

The light-off temperatures are generally lower in case of the u-TWC samples compared to the p-TWC samples. This behavior can be attributed to the higher noble metal content, especially Pd. The values of maximum methane conversion, which are lower by more than 50 °C in case of the u-TWC samples, also reflect this behavior.

3.2. Diesel oxidation catalyst

The total amount of chemical compounds found on the DOC surface is significantly higher than on the TWC surfaces (Table 2). The differences in type and amount of additive elements (P, Ca, Mg, Zn, Fe) detected on the DOC and TWCs are primarily related to (a) differences in the lubricating oil and fuel composition (especially differing additive packages) [4] as well as (b) the higher lubricating oil and fuel consumption.

The carbon concentration detected on the DOC surface seems to be too high for general carbon pollution due to sample storage in ambient air. It is likely that carbon particles typically emitted from the diesel engine also contribute to the signal intensity.

Fig. 4 shows SEM images (×5000, Fig. 4a) and EDX mappings (Fig. 4b–d) of the engine aged DOC. The red areas in Fig. 4b originate from Al of the alumina in the washcoat. The green areas correspond to P originating from different P-containing phases [8]. Yellow areas indicate a mixture of both elements. In contrast to the TWCs, large areas of the washcoat surface are covered by deposits, causing massive fouling. P and Al do not seem to intermix on a detectable scale in EDX; the only clearly visible and consistently yellow areas are the borders of the P deposits. This hints to phosphorous being primarily present in the overlayer. Direct reaction of phosphorous compounds with the washcoat under formation of, e.g. $AlPO_4$ seems to play a minor role.

Fig. 4d shows the P (green) and Zn (red) contaminant distribution on the washcoat surface. The large amount of yellow dots shows an intermixing of P and Zn, which can most likely be attributed to P compounds containing Zn.

Closer inspection of Fig. 4d shows, that practically all areas containing Zn are intermixed with P. On the other hand, some P containing areas do not seem to contain detectable amounts of Zn as is shown by pure green areas without any yellow dots. An overlay of the P EDX mapping with Ca and Mg EDX mappings shows, that these green areas are intermixed with Ca and Mg (not shown in Fig. 4). Eventually, the EDX mappings hint to (a) different P compounds containing varying mixtures of Zn, Ca and Mg and (b) to P compounds with just one cation, e.g. $Zn_3(PO_4)_2$ or $Ca_3(PO_4)_2$.

Fig. 4c shows the Al (red) and Si (green) distribution. This contaminant distribution varies significantly from Zn, Ca and Mg in that Si is almost exclusively detected intermixed with alumina. If at all, only a minor amount of Si is detected within the contaminant overlayer.

Clear information on the Si distribution cannot be deduced from these EDX mappings: (a) is Si directly intermixed with Al forming an alumosilicate compound, or (b) did it diffuse into the washcoat structure, or (c) does it form a thin overlayer on the alumina. Furthermore, it is also unclear if Si is also present underneath the contaminant overlayer or if it is only found within uncovered alumina areas.

In this context, the depth profile analysis (Fig. 5) provides interesting results. After sputtering of the first 100 nm the C concentration is drastically reduced (from 17 to 2 atom%), the Si concentration is slightly reduced. The Zn, P and Al concentrations are increased. Due to the surface sensitivity of XPS, removal of the hydrocarbon overlayer and deposited carbon particles results in an intensity increase of the other elements. This explains the increased Zn and P concentration and probably also contributes to the Al increase. The reduced Si signal intensity is unexpected. A possible explanation could be that Si only forms a thin layer between the washcoat and the thick contaminant overlayer, as observed by Rokosz et al. [6] in taxi TWCs of high mileage. Sputtering of the first 100 nm might therefore remove some of the Si thus decreasing its signal intensity while further increasing the signal intensity of Al.

Increase of the sputter depth results in reduced Zn and P signal intensity due to the removal of the contaminant overlayer. At the same time the Al signal intensity constantly increases since more

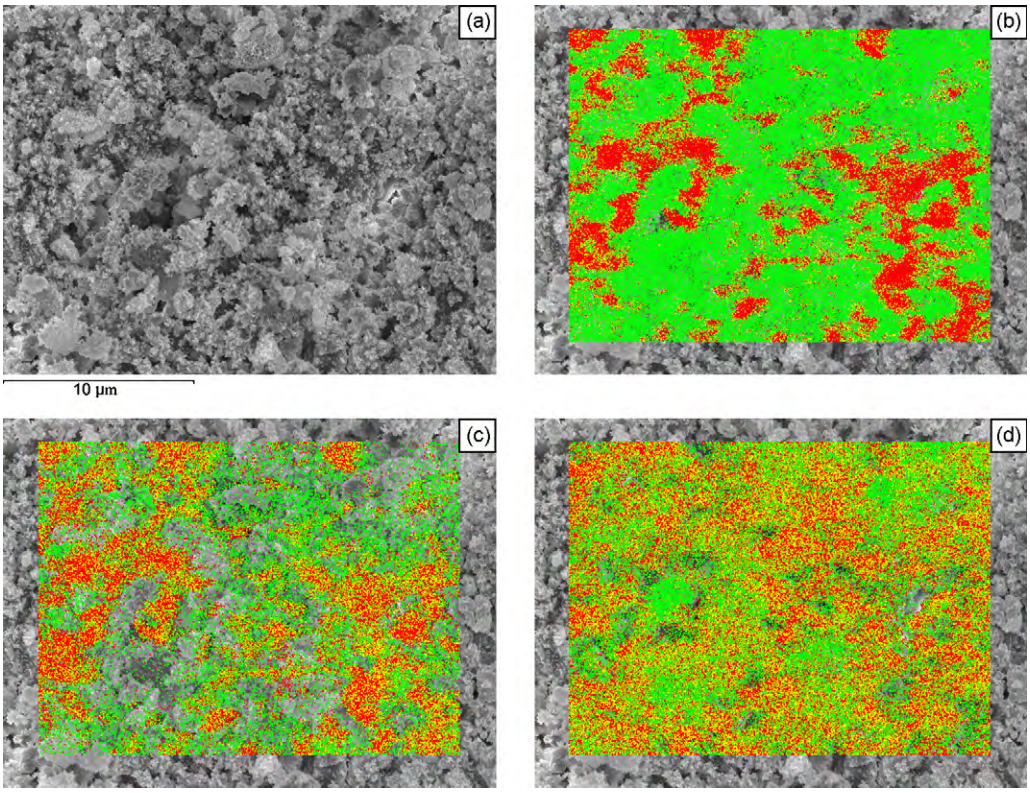

Fig. 4. SEM image of the engine aged DOC (a). EDX mappings of the respective area are shown in (b)–(d). Color code (b): Al: red, P: green. Color code (c): Al: red, Si: green. Color code (d): Zn: red, P: green. Simultaneous signal detection of both respective elements: yellow.

of the washcoat is uncovered. The Si signal intensity marginally increases. This could again be explained by a thin layer between washcoat and overlayer and two contradictory effects. On the one hand, removal of the contaminant overlayer would also uncover more of the Si layer, thus increasing the Si signal intensity. On the other hand, Si might now be sputtered from areas which were formerly uncovered, thus decreasing the Si signal intensity. The Si signal intensity progression seen in Fig. 5 would be a net result of these two effects.

The origin of Si cannot be ascertained for sure. According to BET measurements (Table 1), the SSA of the DOC actually increases, probably due to the large amount of seemingly high porous contaminants, thus not hinting to massive thermal damage. Si diffusion from the cordierite carrier to the washcoat surface can therefore be excluded. A new DOC of the same type was analyzed by XPS and EDX and Si could not be detected within the catalyst, thus also excluding the washcoat as a Si source. In contrast to the TWC experiments, the engine oil could not be analyzed. Therefore, silicone based anti-foaming additives, although generally added in very low quantities, can been present. Additionally, diesel itself, in contrast to gasoline, might also contain low concentrated (~0.001%) silicone based anti-foaming additives [4]. Furthermore, dissolved silicone based engine sealants [6] as well as small dust particles might also contribute to the detected Si.

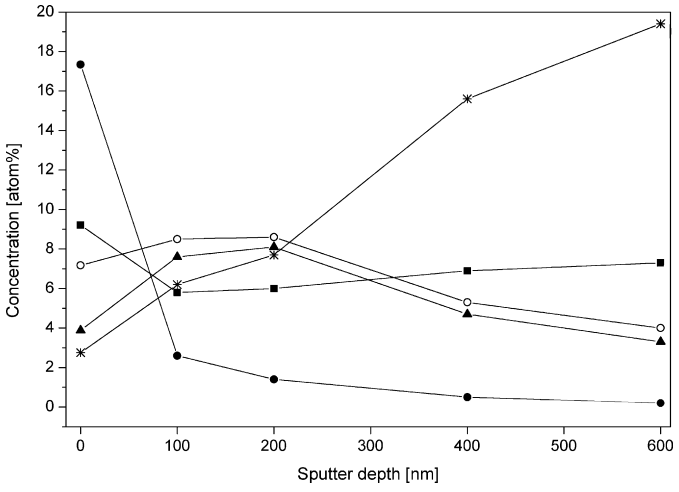

Fig. 5. Sputter depth profile of the engine aged DOC. Assignment of symbols: C (●), Al (✳), Zn (▲), P (○) and Si (■).

The catalytic activity data for the new and engine aged DOC are reported in Fig. 6 in terms of NO and propene conversions. Owing to several *m*/*z* overlaps, only a quantification of the MS data corresponding to *m*/*z* 30 and *m*/*z* 42 is feasible. It is obvious that chemical aging has a dramatic effect on the catalytic performance of the DOC. The difference in light-off temperature for propene conversion is by ca. 70 °C in favor of the new DOC (Table 3), but both samples attain full conversion.

In case of the new DOC, NO conversion starts at about 170 °C. The maximum conversion of 41% is reached at about 215 °C and this conversion level is kept almost constant till 260 °C (Table 3). For the aged DOC, NO conversion starts about 70 °C higher and maximum conversion of 31% is reached at about 250 °C. Thereafter, the conversion is immediately but gradually reduced. The depletion of NO activity has been observed on both DOC and TWC catalysts [14,15]. The inhibition of NO reduction has been attributed to the influence of the oxygen coverage over the noble metal, which appears negligible until propene is completely converted and becomes important at propene full conversion [14]. From this point on, the reduction of NO is hindered and NO oxidation to NO_2 occurs [16]. Aging causes the activity window of the DOC to narrow and in fact only a sharp maximum of conversion is observed followed by the continuous loss of activity. The

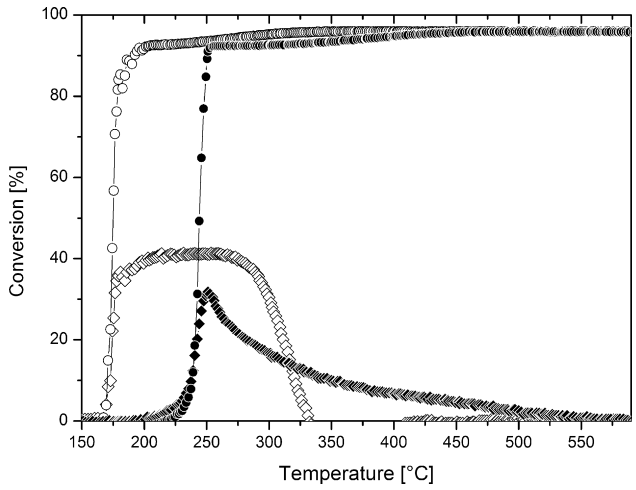

Fig. 6. Catalytic activity data for new and engine aged DOC for propene (○) and NO (◇) conversion. Open and filled symbols represent new and aged catalysts, respectively.

difference in activity between the new and engine aged DOC can most likely be attributed to the heavy chemical aging. This seems to be a non-specific effect, influencing the conversion efficiency of all analyzed gas compounds. Nevertheless, it cannot be excluded that some sintering of PM particles also occurred, even though the aged DOC does not show any loss in SSA. This effect might also contribute to the loss in catalytic activity.

4. Summary and conclusion

Aging effects were characterized for a 35,000 km vehicle aged pre- and underfloor three-way catalyst from a bifuel passenger car as well as for an engine aged diesel oxidation catalyst. The impact of the aging phenomena on the catalytic activity was assessed via conversion experiments employing model exhaust gases. For comparison, the conversion efficiency of the respective degreened (TWC) and new (DOC) catalyst was also analyzed.

The p-TWC had experienced massive thermal aging. Its CO light-off temperature increased by about 110 °C and the maximum CO conversion attained was slightly reduced. The light-off temperature for methane remained almost unchanged, but above 325 °C a substantial loss of CH_4 conversion was detected. Given the collapse of the p-TWC structure, it was surprising that the catalyst still showed such relatively high activity.

The u-TWC experienced some chemical aging, primarily consisting of P compounds as well as minor thermal aging. As was the case for the p-TWC the CO light-off temperature was also increased by about 110 °C, but in contrast to the vehicle aged p-TWC its activity towards methane was substantially unaltered.

A clear differentiation between the effect of chemical and thermal aging on conversion efficiency does not appear to be straightforward in case of the TWC samples. Only the catalytic activity with respect to the methane conversion was influenced by the type of aging. Whereas chemical aging does not seem to affect the catalyst performance, thermal aging substantially deteriorates it.

The engine aged diesel oxidation catalyst exhibited strong chemical aging primarily with Zn, P and Si. Si seemed to be deposited between the washcoat and the P and Zn containing contaminant overlayer. No unusual thermal aging was detected. Both propene and NO light-off activities were strongly affected compared to the new catalyst.

References

[1] A. Takigawa, A. Matsunami, N. Arai, Energy 30 (2005) 461.
[2] A. Winkler, P. Dimopoulos, R. Hauert, C. Bach, M. Aguirre, Appl. Catal. B 84 (2008) 162.
[3] J. Franz, J. Schmidt, C. Schoen, M. Harperscheid, S. Eckhoff, M. Roesch, J. Leyrer, SAE Paper 2005-01-1097.
[4] R. van Basshuysen, F. Schaefer, Handbuch Verbrennungsmotoren - 2. verbesserte Auflage, Friedr. Vieweg & Sohn Verlagsgesellschaft mbH, Braunschweig/Wiesbaden, 2002, pp. 701–738.
[5] D.D. Beck, J.W. Sommers, C.L. Di Maggio, Appl. Catal. B 11 (1997) 257.
[6] M.J. Rokosz, A.E. Chen, C.K. Lowe-Ma, A.V. Kucherov, D. Benson, M.C. Paputa Peck, R.W. McCabe, Appl. Catal. B 33 (2001) 205.
[7] A.K. Neyestanaki, F. Klingstedt, T. Salmi, D.Y. Murzin, Fuel 83 (2004) 395.
[8] M.L. Granados, C. Larese, F. Cabello Galisteo, R. Mariscal, J.L.G. Fierro, R. Fernandez-Ruiz, R. Saguino, M. Luna, Catal. Today 107–108 (2005) 77.
[9] J. Andersson, M. Antonsson, L. Eurenius, E. Olsson, M. Skoglundh, Appl. Catal. B 72 (2007) 71.
[10] V. Kröger, M. Hietikko, D. Angove, D. French, U. Lassi, A. Suopanki, R. Laitinen, R.L. Keisik, Top. Catal. 42–43 (2007) 409.
[11] Y. Song, S. Choi, C. In, G. Yeo, SAE Paper 2005-01-1096.
[12] D.E. Angove, N.W. Cant, D.H. French, K. Kinealy, Appl. Catal. A 194–195 (2000) 27.
[13] J.F. Moulder, W.F. Stickle, P.E. Sobol, K.D. Bomben, in: J. Chastian (Ed.), Handbook of X-Ray Photoelectron Spectroscopy, Perkin-Elmer Corporation, Minnesota, 1992
[14] R. Burch, J.A. Sullivan, T.C. Watling, Catal. Today 42 (1998) 13.
[15] J.A. Bota, M.A. Gutierrez-Ortiz, M.P. Gonzalez-Marcos, J.A. Gonzalez-Marcos, J.R. Gonzalez-Velasco, Appl. Catal. B 32 (2001) 243.
[16] M. Crocoll, S. Kureti, W. Weisweiler, J. Catal. 229 (2005) 480.